REPORT

TOPOLOGICAL OPTICS

Tunable topological charge vortex microlaser

Zhifeng Zhang[1], Xingdu Qiao[1], Bikashkali Midya[2], Kevin Liu[2], Jingbo Sun[3], Tianwei Wu[2], Wenjing Liu[2], Ritesh Agarwal[2], Josep Miquel Jornet[4], Stefano Longhi[5,6], Natalia M. Litchinitser[3], Liang Feng[2,1]*

The orbital angular momentum (OAM) intrinsically carried by vortex light beams holds a promise for multidimensional high-capacity data multiplexing, meeting the ever-increasing demands for information. Development of a dynamically tunable OAM light source is a critical step in the realization of OAM modulation and multiplexing. By harnessing the properties of total momentum conservation, spin-orbit interaction, and optical non-Hermitian symmetry breaking, we demonstrate an OAM-tunable vortex microlaser, providing chiral light states of variable topological charges at a single telecommunication wavelength. The scheme of the non–Hermitian-controlled chiral light emission at room temperature can be further scaled up for simultaneous multivortex emissions in a flexible manner. Our work provides a route for the development of the next generation of multidimensional OAM-spin-wavelength division multiplexing technology.

I n the digital era of proliferating connections between pervasive endpoints, the tremendously growing aggregated data traffic motivates the development of innovative optical communication technologies to sustain the required massive increase in information capacity. The current information infrastructure based on wavelength and time division multiplexing—together with other degrees of freedom of light, including the amplitude, polarization, and phase—is nevertheless approaching a bottleneck. Fortunately, the full-vector nature of light provides another information dimension—namely, the angular momentum—to ease the upcoming information crunch. Whereas the spin angular momentum (SAM) associated with the circular polarization of light is limited by two states ($\sigma = \pm 1$), the orbital angular momentum (OAM) of a vortex beam with an azimuthal phase dependence ($E \sim e^{il\varphi}$, where E is the complex electric field distribution, characterized by the topological integer $l = 0, \pm 1, \pm 2...$, and φ is the azimuthal angle) (1, 2) creates a dimension of unlimited spatially distinguishable channels for data transmission. In addition to their potential for optical communication (3–6), optical vortex beams carrying OAM have also revolutionized several applications in the fields of optical manipulation (7, 8), imaging and microscopy (9, 10), and quantum information processing (11, 12).
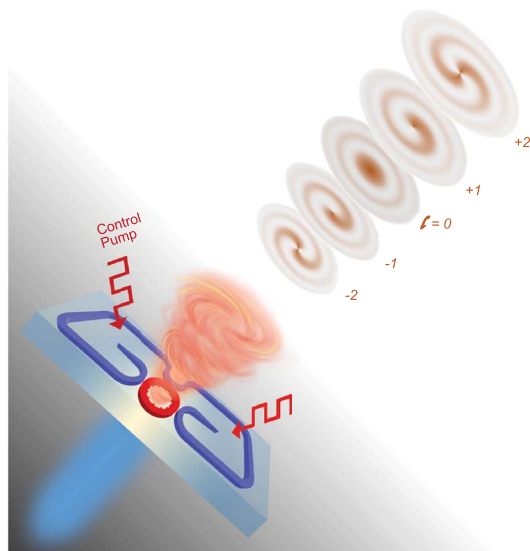
Dynamically tunable vortex light sources have become essential to bring into reality these emerging photonic technologies based on the OAM degree of freedom. Traditional bulk optical components such as spiral phase plates and forked holograms (2, 13)—or recently developed planar optical components, including various metasurfaces (14–17) and silicon resonators (18), used for OAM beam generation—require an external input beam that originates from a separate light source. Chip-scale microlasers offer a more compact and robust solution to obtain highly pure coherent vortex modes and have been recently investigated extensively (19–21). However, the demonstrated miniaturized vortex lasers at telecommunication wavelengths so far lack reconfigurability, limited by their output of a predefined polarized OAM state per wavelength (19, 20). Nevertheless, the ongoing effort of OAM-SAM-wavelength (3–6) division multiplexing for multidimensional high-capacity information processing requires flexible generation and versatile manipulation of different OAM and SAM states at the same wavelength, which is not yet accessible by state-of-the-art microscale devices.

We used the transverse spin and OAM interaction to precisely maneuver the chiral light states in microring lasers. Additionally, total angular momentum conservation allows further tuning of the topological charge. The ability to simultaneously and cohesively manipulate both the SAM and OAM degrees of freedom can couple the local spin with orbital oscillation of optical cavity modes, leveraging richer functionalities in vortex light generation (22, 23). Spin-orbit coupling can enable effective control of the OAM handedness arising from the chiral symmetry of $\pm|l|$ wave functions, featuring the ability to flexibly generate multivortex emissions of variable $|l|$ OAMs in the full angular momentum space. Although it is straightforward to switch the chirality depending on the direction of input light in a passive microring resonator (18), a sophisticated active, robust strategy is required to selectively break the chiral symmetry that is intrinsically associated with a microring laser, yielding flexible control of spin-orbit interaction. Optical control of spin-orbit interaction and its induced chiral light emission have been demonstrated through spin-polarized gain generation in a semiconductor polaritonic system (21); however, in such a device a cryogenic environment is required, which is not suitable for practical integration in current information systems. To create a robust yet reconfigurable

Fig. 1. Schematic of non–Hermitian-controlled vortex microlaser. The non-Hermitian interaction mediated by the externally applied control pump on the bus waveguide can flexibly be switched for the emission of OAM states with desirable chirality from the spin-orbit engineered microring.

spin-orbit coupling in an ambient-temperature environment, we developed a microlaser system in which spin-orbit interaction is controlled by an externally applied non-Hermitian coupling between the cavity modes (Fig. 1). Strategic non-Hermitian symmetry breaking facilitates the lifting of degeneracy between two spin-orbit coupled states, of which the spin is locked to the orbit direction, in a controllable manner and favors the lasing of an OAM state of desirable chirality. The spin-orbit interaction, together with the conservation of the total angular momentum, is further exploited to alter the emitted OAM state by converting the SAM into OAM, introducing additional tunability with variable topological charges at the same wavelength. This scheme can be further scaled up to simultaneously generate multiple laser vortices with an imaginary gauge (24, 25) conducted in the coupled system (26).

We considered a microring resonator supporting the two degenerate clockwise (↻) and counterclockwise (↺) whispering gallery modes (WGMs) on a III-V semiconductor platform with a 200-nm-thick InGaAsP multiple quantum well layer, coupled with an additional bus waveguide of InGaAsP with two control arms, which enables the indirect coupling between the two modes (Figs. 1 and 2). By finely tuning the aspect ratio of the cross-section geometry of the waveguide, the transverse spin in the evanescent tail of guided light is engineered to be 1, which is achieved with equal amplitudes of the radial and azimuthal components of the electric field (26). The absolute value of transverse spin generated in this scheme cannot exceed 1. The spin-orbit interaction consequently couples the right-hand (↓) and left-hand (↑) circular polarizations with the ↺ and ↻ modes, respectively, leading to spin-orbit locking for the light circulating in the microring. The degeneracy between these two countercirculating states is broken by introducing non-Hermitian mode coupling by means of the bus waveguide. By optically pumping one of the waveguide arms to create gain (generated through pumping) and loss (intrinsic material loss without pumping) contrast, an effective asymmetric coupling between the counterpropagating WGMs in the microring is obtained. The Hamiltonian of the non-Hermitian controlled microring resonator can effectively be described as

$$H_{\text{eff}} = \begin{pmatrix} \omega_{\circlearrowleft} & \kappa e^{-\gamma} e^{+\gamma_L} \\ \kappa e^{-\gamma} e^{+\gamma_R} & \omega_{\circlearrowright} \end{pmatrix} \quad (1)$$

where $\omega_{\circlearrowleft}$ and $\omega_{\circlearrowright}$ are the eigen frequencies of the two degenerate modes; κ denotes the coupling between the cavity modes without any gain or loss in the bus waveguide; $-\gamma$ describes the single pass attenuation due to the intrinsic material loss; and $+\gamma_R$ and $+\gamma_L$
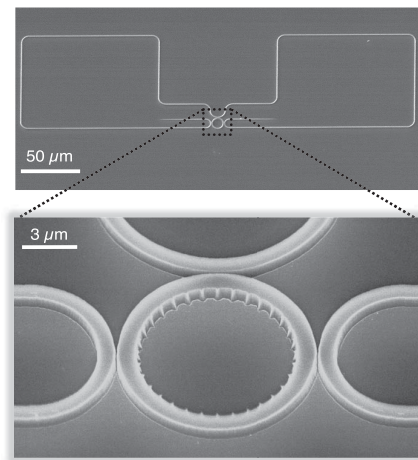

Fig. 2. Scanning electron microscope images of the tunable vortex microlaser. On an InGaAsP multiple quantum well platform, the microlaser consists of a main microring cavity coupled to an external feedback loop that enables the on-demand chiral control through selective pumping and thus enforces the unidirectional coupling between the two circulating modes in the microring. The angular grating is patterned on the inner sidewall of the microring to produce the vortex laser emission of variable topological charges.
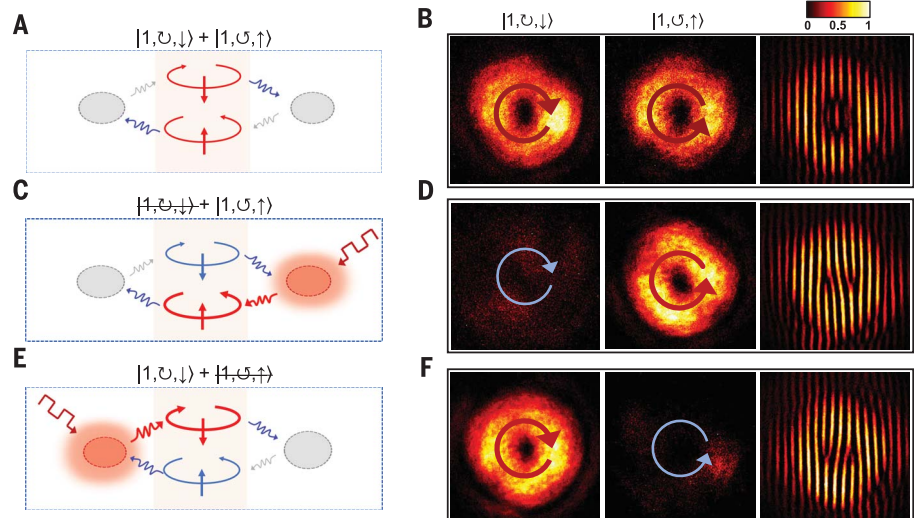
Fig. 3. Non-Hermitian chiral interactions and experimental characterization of the lasing emission.
(**A**) In the absence of non-Hermitian interaction, both the cavity modes represented by $||l|, \text{sgn}(l), \sigma\rangle$—with $\text{sgn}(l) = \pm 1$ denoting the CCW (↺) and CW (↻) oscillations, respectively, and $\sigma = \pm 1$ denoting the left (↑) and right (↓) circularly polarized light—are favored for lasing action. (**B**) Corresponding experimentally measured output emissions and off-center self-interference pattern of both the states. (**C** and **D**) Lasing emission of left-chiral mode measured after the introduction of non-Hermitian interaction applied by the right-side control pump. (**E** and **F**) Lasing emission of right-chiral mode measured after reversing the non-Hermitian interaction applied by the left-side control pump. The shaded rectangular area at left denotes the microring cavity, and the shaded elliptical areas indicate non-Hermitian control arms. The red and gray arrows outside the cavity denote the gain and loss feedback, respectively, and the blue arrows represent energy outcoupled from the cavity into the environment. Because of the unidirectional gain feedback, the red cavity mode is selectively favored for chiral lasing action, whereas the blue cavity mode is suppressed.

represent the single pass amplification from the optical pumping applied to the right and left control arms, respectively. This effective Hamiltonian can also be transformed into a parity-time symmetric-like form (27) by using the basis of $\omega_{\circlearrowleft} + i\omega_{\circlearrowright}$ and $\omega_{\circlearrowleft} - i\omega_{\circlearrowright}$ states (26). In the absence of optical pumping on the control arm ($\gamma_L = \gamma_R = 0$), the overall coupling strength between ↻ and ↺ modes approaches zero because of the strong intrinsic material loss of the InGaAsP multiple quantum well ($\gamma \gg 1$) (Fig. 3A). When the left (or right) control arm is selectively pumped, the intrinsic material loss on the left (or right) is then overcome by net optical gain, $\gamma_L > \gamma$ (or $\gamma_R > \gamma$). However, the unpumped right (or left) side of the waveguide remains lossy. Because of spin-orbit locking, selective pumping results in a unidirectional coupling between the ↻ and ↺ modes, breaking the chiral symmetry and facilitating an effective means to controlling the chirality of the mode (Fig. 3, C and E). Under this condition, the microlaser effectively operates at an exceptional point (19).
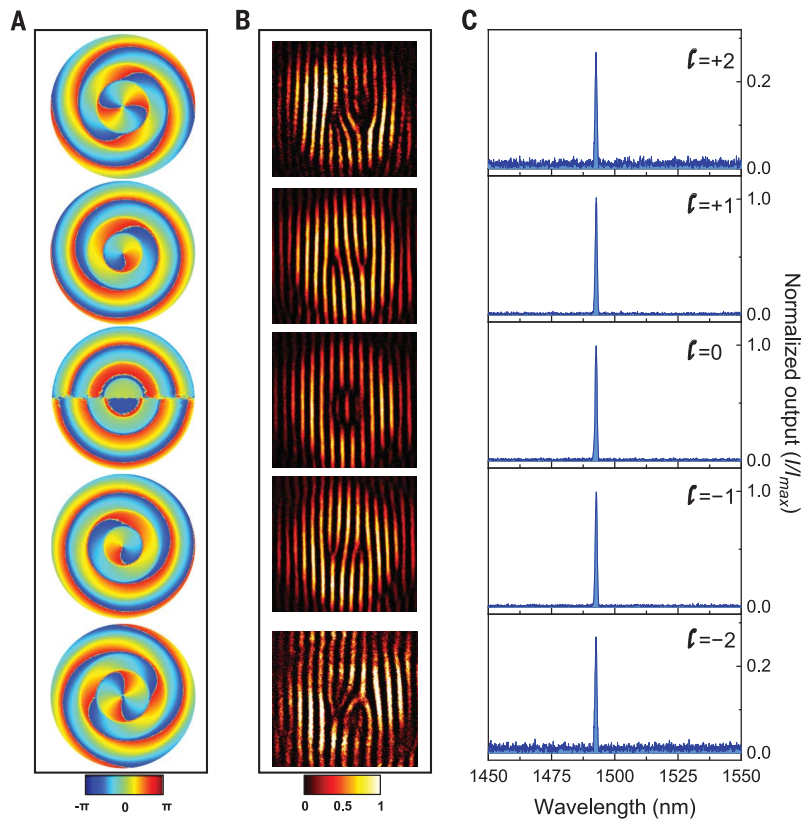
Fig. 4. Experimental characterization of different OAM states at a fixed wavelength. (**A**) Simulated phase distributions of OAMs of charges $l = 0, \pm1,$ and ±2, showing the helical phase winds $2l\pi$ around the center. The OAMs of the lower three orders were achieved through spin-orbit locking, and higher-order OAMs were obtained through the spin-to-orbit coupling: $(\sigma, l) = (\pm1, \pm1)$ to $(\sigma, l) = (0, \pm2)$. In both cases, the chiral symmetry was broken by controllable non–Hermitian mode coupling. (**B**) Corresponding experimental results showing the off-center self-interference patterns (images are enhanced for better visualization). Although no notable fringe mismatch was observed for the $l = 0$ state, a pair of inverted forks were observed for nonzero OAMs. A single fringe splits into two or three, indicating a phase wind of 2π or 4π around the center singularity point, confirming the OAM of $|l| = 1, 2$, respectively. The forks associated with opposite chirality were in opposite directions. (**C**) Measured lasing spectra show all five OAM lasing peaks located at 1492.6 nm, implying that the vortex microlaser can generate single-frequency vortex beams of variable OAMs simultaneously.

Unidirectional emission is robust against instabilities induced by nonlinearities above the laser threshold (*28*) and is essential to realize our single-frequency microlaser with reconfigurable OAM through spin-orbit coupling.

The non-Hermitian controlled microlaser was designed so that the angular momentum carried by the WGM inside the resonator is extracted into free space by introducing periodic angular scatters on the inner sidewall (Fig. 2). The angular scatters are located at $\theta_q = 2\pi q/M$ and carry a local phase of $\varphi_{\text{local},q} = 2\pi Cq(N - M)/M$, where $q \in \{0, M-1\}$; $C = \text{sgn}(\sigma)$ for the $\circlearrowleft$ and $\circlearrowright$ modes, respectively; and N is the order of the WGM. By accounting for the rotation of local coordinates with respect to the global coordinate, the extracted global phase can be expressed as $\varphi_{\text{global},q} = 2\pi C[q(N - M) - q]/M$. Consequently, the linearly varying phase distribution creates an OAM emission with a topological charge of $l = C(N - M - 1)$ and a

total angular momentum of $J = C(N - M)$. The corresponding vortex emission, containing both SAM and OAM as well as their associated chirality, can be represented as $||l|, \text{sgn}(l), \sigma\rangle$. In our experiment, the microlaser cavity has a diameter of 7 μm and a width of 0.65 μm, which supports a WGM on the order of $N = 34$ and scatter number $M = 32$ for a total angular momentum of $|J| = 2$.

To better configure the non–Hermitian-controlled chirality and its resulting spin-orbit interaction, two synchronized pump beams from a nanosecond laser were projected: one onto the microlaser cavity to carry out the lasing and the other to selectively pump one of the control arms to manipulate the chirality of the lasing (*26*). The chiral symmetry of the system was observed in the absence of a control pump (Fig. 3A). The emission from the resonator showed right- and left-handed circularly polarized components

of nearly balanced intensities without a net spin angular momentum (Fig. 3B). This reveals the absence of net nonzero angular momentum resulting from the coexistence of the two degenerate $\circlearrowleft$ and $\circlearrowright$ modes. To probe the vortex nature of laser radiations, the emitted beam was split into two identical beams that were subsequently interfered with a slight offset in the horizontal direction. The acquired interferogram shows no notable fringe mismatch or discontinuity, indicating no phase winding near the center of the beam, which confirms a net-zero OAM charge (Fig. 3B). By contrast, when the control beam was switched on while illuminating only the right control arm (Fig. 3C), unidirectional laser oscillation arose in the $\circlearrowright$ mode. The emission of nearly perfect left-handed circular polarization was consequently observed, revealing the unidirectional power circulation of the $\circlearrowright$ mode inside the microring and spin-orbit locking. Because of phase singularity, the phase distribution changes drastically near the center of the emitted laser beam while maintaining relatively uniform distribution at outer regions. Therefore, the corresponding self-interference pattern shows a pair of inverted forks, verifying the topological charge of OAM laser emissions. In each fork, a single fringe splits into two, corresponding to an OAM charge of +1 (Fig. 3D). Similarly, when the control beam was only applied onto the left control arm (Fig. 3E), a nearly perfect right-handed circularly polarized emission was observed instead, demonstrating the non–Hermitian-controlled switching of chirality through spin-orbit locking. The orientations of the forks were reversed compared with the previous condition, in which the single fringe still splits into two but in the opposite direction, verifying an OAM charge of –1 (Fig. 3F).

Additional tunability of the OAM charge through the conservation of the total angular momentum in the spin-to-orbit conversion was demonstrated with the vortex microlaser by using a radial polarizer that preserves the rotational symmetry of the emitted laser beam (*26*). The radial polarizer allows the transmission of only radially polarized light and thus converts circularly polarized light into a linearly polarized beam in a polar coordinate. Because the radial polarizer does not break the rotational symmetry, the total angular momentum, $J = l + \sigma$, of light must remain conserved. For a given J, l can therefore be controlled through the manipulation of σ. The new OAM states with $l = \pm2$ were achieved after the transfer of $\sigma = \pm1$ SAMs into the demonstrated $l = \pm1$ OAMs, respectively, when the laser beam was passed through the polarizer. The self-interference interferograms were captured to analyze the vortex reconfiguration of the emitted beams. A pair of inverted forks with three fringes were observed, revealing a

phase winding of 4π at the center, which confirmed the OAM charge $l = \pm 2$ (Fig. 4, A and B, top and bottom). Altogether, the non–Hermitian-controlled vortex microlaser is capable of producing five different OAM states ranging in $l = -2, -1, 0, +1, +2$ in a reconfigurable manner. The lasing of all these OAM states occurred at a "single" wavelength at 1492.6 nm (Fig. 4C), potentially providing five spatial channels for information modulation and communication (26). The switching time of spin-orbit coupling is in principle limited by the semiconductor optical response, with the potential to reach ultrafast OAM switching in the picosecond scale (29), so that our reconfigurable OAM microlaser, besides emitting at a fixed wavelength, is much faster than those based on thermo-optic control of WGM resonances (microsecond to millisecond time scales). Further, our non-Hermitian spin-orbit mode control scheme is scalable by applying an imaginary gauge (24, 25) to cascade sequential microrings to simultaneously generate multiple laser vortices; experimental results are given in (26).

Our tunable OAM microlaser is capable of emitting vortex beams of five different topological charges at room temperature. The non-Hermitian manipulation of chiral spin-orbit interaction offers fundamentally new functionality of controllable vortex light emission in a scalable way. The non-Hermitian control of spin-orbit interactions and thus OAM emissions is general and compatible with conventional electrical pumping schemes in which standard p-i-n semiconductor configurations are exploited for current injection to excite optical gain (30). The toolbox of generating various vortex light at a single wavelength holds the promise for future development of multidimensional OAM-SAM-wavelength division multiplexing for high-density data transmission in classical and quantum regimes. Additionally, dynamic switching between different OAM modes in time can further increase the security of wired and wireless communication networks (26).

REFERENCES AND NOTES

1. L. Allen, M. W. Beijersbergen, R. J. C. Spreeuw, J. P. Woerdman, *Phys. Rev. A* **45**, 8185–8189 (1992).
2. A. M. Yao, M. J. Padgett, *Adv. Opt. Photonics* **3**, 161–204 (2011).
3. J. Wang *et al.*, *Nat. Photonics* **6**, 488–496 (2012).
4. N. Bozinovic *et al.*, *Science* **340**, 1545–1548 (2013).
5. I. M. Fazal *et al.*, *Opt. Lett.* **37**, 4753–4755 (2012).
6. A. E. Willner *et al.*, *Adv. Opt. Photonics* **7**, 66–106 (2015).
7. H. He, M. E. J. Friese, N. R. Heckenberg, H. Rubinsztein-Dunlop, *Phys. Rev. Lett.* **75**, 826–829 (1995).
8. M. Padgett, R. Bowman, *Nat. Photonics* **5**, 343–348 (2011).
9. L. Torner, J. Torres, S. Carrasco, *Opt. Express* **13**, 873–881 (2005).
10. C. Maurer, A. Jesacher, S. Bernet, M. Ritsch-Marte, *Laser Photonics Rev.* **5**, 81–101 (2011).
11. A. Mair, A. Vaziri, G. Weihs, A. Zeilinger, *Nature* **412**, 313–316 (2001).
12. J. Leach *et al.*, *Science* **329**, 662–665 (2010).
13. D. Naidoo *et al.*, *Nat. Photonics* **10**, 327–332 (2016).
14. N. Yu *et al.*, *Science* **334**, 333–337 (2011).
15. D. Lin, P. Fan, E. Hasman, M. L. Brongersma, *Science* **345**, 298–302 (2014).
16. M. I. Shalaev *et al.*, *Nano Lett.* **15**, 6261–6266 (2015).
17. C. W. Qiu, Y. Yang, *Science* **357**, 645–645 (2017).
18. X. Cai *et al.*, *Science* **338**, 363–366 (2012).
19. P. Miao *et al.*, *Science* **353**, 464–467 (2016).
20. W. E. Hayenga *et al.*, *ACS Photonics* **6**, 1895–1901 (2019).
21. N. Carlon Zambon *et al.*, *Nat. Photonics* **13**, 283–288 (2019).
22. K. Y. Bliokh, F. J. Rodríguez-Fortuño, F. Nori, A. V. Zayats, *Nat. Photonics* **9**, 796–808 (2015).
23. Z. Shao, J. Zhu, Y. Chen, Y. Zhang, S. Yu, *Nat. Commun.* **9**, 926 (2018).
24. S. Longhi, L. Feng, *APL Photon.* **3**, 060802 (2018).
25. S. Longhi, *Ann. Phys.* **530**, 1800023 (2018).
26. Materials, methods, and additional information are available as supplementary materials.
27. L. Feng, R. El-Ganainy, L. Ge, *Nat. Photonics* **11**, 752–762 (2017).
28. S. Longhi, L. Feng, *Photon. Res.* **5**, B1 (2017).
29. C. Huang *et al.*, *Science* **367**, 1018–1021 (2020).
30. J. Zhang *et al.*, *Nat. Commun.* **9**, 2652 (2018).

SUPPLEMENTARY MATERIALS

science.sciencemag.org/content/368/6492/760/suppl/DC1
Supplementary Text
Figs. S1 to S10
References (31–35)

15 January 2020; accepted 19 March 2020
10.1126/science.aba8996

Science

Tunable topological charge vortex microlaser

Zhifeng Zhang, Xingdu Qiao, Bikashkali Midya, Kevin Liu, Jingbo Sun, Tianwei Wu, Wenjing Liu, Ritesh Agarwal, Josep Miquel Jornet, Stefano Longhi, Natalia M. Litchinitser and Liang Feng

Optical vortices on demand

Light has several degrees of freedom (wavelength, polarization, pulse length, and so on) that can be used to encode information. A light beam or pulse can also be structured to have the property of orbital angular momentum, becoming a vortex. Because the winding number of the vortex can be arbitrary, the channel capacity can be expanded considerably. Zhang *et al.* and Ji *et al.* developed nanophotonic-based methods for generating and electrically detecting light with arbitrary orbital angular momentum, a goal that has remained an outstanding challenge so far (see the Perspective by Ge). The nanophotonic platform provides a route for developing high-capacity optical chips.

Science, this issue p. 760, p. 763; see also p. 707